High-performance piezoelectric nanogenerator based on low-entropy structured nanofibers for multi-mode energy harvesting and self-powered UV photodetector

Wancheng Qin¹, Peng Zhou¹, Xinyu Xu¹, Chuanwei Huang², Gopalan Srinivasan³, Yajun Qi^{1*}, Tianjin Zhang^{1*}

- Ministry of Education Key Laboratory for Green Preparation and Application of Functional Materials, Hubei Provincial Key Laboratory of Polymers, Collaborative Innovation Center for Advanced Organic Chemical Materials Co-constructed by the Province and Ministry, School of Materials Science and Engineering, Hubei University, Wuhan 430062, PR China
- Shenzhen Key Laboratory of Special Functional Materials, College of Materials Science and Engineering, Shenzhen University, Shenzhen, 518060, China
- 3. Physics Department, Oakland University, Rochester, Michigan 48309, USA Corresponding authors: yjqi@hubu.edu.cn (Y. J. Qi) and zhangtj@hubu.edu.cn (T. J. Zhang)

Abstract

Piezoelectric nanogenerators (PNG) based on flexible inorganic nanomaterials have attracted significant attention due to their superior flexibility and high output performance. However, achieving high inorganic nanomaterial dispersibility in piezoelectric composites is still a challenge for enhancing the electrical outputs. We have implemented a method for increasing the dispersibility of zinc oxide (ZnO) nanoparticles implanted in poly(vinylidene fluoride trifluoroethylene) (P(VDF-TrFE)) composites by generating a D-phenylalanine (D-phe) chelate with ZnO nanoparticles. The flexible electronic devices assembled with the chelate D-phe@ZnO/P(VDF-TrFE) composites possess multifunctionality and superior electrical outputs. D-phe@ZnO/P(VDF-TrFE) PNG exhibits a maximum output voltage of 33 V and a power density of 8.5 μW/cm², which are significant improvement compared to pure P(VDF-TrFE) and ZnO/P(VDF-TrFE) composites PNGs. Output voltage of 25 V can be obtained from the designed PNG by finger tapping, and provided sufficient power to light 15 LEDs. Furthermore, the high-sensitivity and fast-response to the ultraviolet (UV) illumination of the designed composites demonstrate their potential application

of the self-powered UV photodetectors. Such a nanogenerator has multiple application modes, indicating great potential in the application of the piezo-phototropic technology.

Keywords

D-phe@ZnO chelate nanowires, P(VDF-TrFE), low-entropy structured nanofibers, piezoelectric nanogenerator, self-powered UV photodetector

1. Introduction

With the acute need for the development of informatization and emerging electronic industries, wearable devices have become important for scientific research and industrial transformation in countries around the world¹⁻³. However, a common disadvantage of traditional wearable devices (such as wristwatches⁴ and eyeglasses⁵) is that they all need to have rechargeable batteries to provide power, which limits their sustainability and longevity⁶. In addition, the size and weight of the battery further limit the miniaturization of portable devices. Therefore, efforts are in progress to come up with alternatives to operate these wearable electronic devices by directly using the energy generated by human motion to achieve their "self-powered" property and sustainability^{7, 8}. Since human activities produce mechanical energy, the electromechanical conversion characteristics of piezoelectric materials can be used to realize the collection of mechanical energy and its conversion to electrical energy^{9, 10}. Using this ubiquitous biomechanical energy source is one of the most reliable strategies for generating electricity for wearable devices.

Polyvinylidene difluoride (PVDF) and its copolymers with biocompatibility have been favored by many researchers due to their superior piezoelectricity and flexibility. The inorganic piezoelectric nanofillers have been employed to incorporate into the polymer matrix to further enhance the output of the nanogenerator¹¹. Due to the high aspect ratio of the inorganic nanostructures, the dispersibility of the nanofillers is of great importance for improving the electrical performance. As demonstrated in the organic/inorganic composite nanofibers, the clustering of nanoparticles further

deteriorates the degree of order of the nanofibers, causing many defects, which limit the output of the device^{12, 13}. Fortunately, poly(methyl methacrylate) (PMMA)¹⁴ and dopamine (DA)¹⁵ have been used as surface modifiers and significantly enhanced the dispersion of nanoparticles. Compared with the use of polymers for surface modification, the chelate skeleton to disperse nanoparticles has the advantage of simple process and low cost^{16, 17}. As far as we know, using the chelate framework to disperse the inorganic nanoparticles to enhance the output of nanogenerators has not been reported. Moreover, the chelates would further increase the degree of order of the nanofibers and thus improve the crystalline and volume fraction of the ferroelectric polar phase in PVDF and thus further enhance the electrical outputs.

Furthermore, because of their potential applications in intelligent equipment and flexible electronics, multifunctional electronic devices have gotten a lot of interest. Integrating the flexible nanogenerator into a photodetector provide a solution for the limitation of the current normal sensors such as regular replacement of batteries and boosted structural complexity, etc.. Sultana *et al.*¹⁸ reported that methylammonium lead iodide and PVDF composite film can be used for photoactive piezoelectric energy harvesters and photodetectors. In piezo-phototronics technology, the piezoelectric nanogenerator's simultaneous mechanical energy harvesting and light detecting capacity is also a promising aspect.

To our knowledge, no attempt has been made to include D-phe@ZnO chelated nanowires into poly(vinylidene fluoride trifluoroethylene) P(VDF-TrFE) to make it appropriate for mechanical energy harvesting, photodetector application, and hybridize photoactive piezoelectric energy harvester. In this report, D-phe@ZnO chelated nanowires were designed by using D-phenylalanine (D-phe) and ZnO nanoparticles, which can form a secondary electric field during the electrospinning process so that the nanofibers are stably generated and evenly arranged on the spinning drum. The nanofiber film with high orientation and compact arrangement was obtained. D-phe@ZnO/P(VDF-TrFE) composite PNG is capable of generating a maximum voltage output of 33 V, a current output of 4.1 μA, and its output power density as high as 8.5 μW/cm². With a light finger tapping, the output voltage can

reach 25 V and can light up 15 LEDs. As a result, PNGs have a wide range of applications as a power source for portable micro-nano devices and wearable electronics. It can also detect ultraviolet (UV) light based on considerable changes in output voltages and currents under UV illumination, paving the way for it to be used as a self-powered UV photodetector in the future.

2. Experimental and characterization

2.1 Materials

ZnO (30 ± 10 nm, 99.9 %), D-phenylalanine (165.19 g/mol) and Tris (hydroxymethyl) aminomethane, (Tris, ≥ 99.9 % (T)) were acquired from Aladdin (China). P(VDF-TrFE) (70/30 mol.%) was supplied by Kunshan Hisense Electronic Co. Ltd. N, N-dimethylformamide (DMF, 99.7%, Mw: 73.09), anhydrous alcohol (≥ 99.7 %) and Acetone (99.5%, Mw: 58.08) were procured from Sinopharm Chemical Reagent Co., Ltd. (Shanghai, China). Without additional purification, all chemicals and reagents were utilized. Indium tin oxide (ITO) coated polyethylene terephthalate (PET) substrates were purchased from Sigma-Aldrich.

2.2 Preparation of D-phe@ZnO chelate nanowires

To form D-phe@ZnO chelate nanowires, 25 mg Tris was dissolved into 20 mL deionized (DI) water to form Tris buffer solution (pH = 8.5). Then 100 mg ZnO was added and the solution was sonicated for 60 minutes to ensure that the ZnO nanoparticles were evenly dispersed. Afterward, 100 mg D-phe was added to the above solution and magnetically stirred at 70 °C for 24 hours. During the stirring process, D-phe@ZnO chelate nanowires were formed due to the complexation of D-phe on zinc ions. After centrifugation at 1,000 rpm for 5 minutes, it was repeatedly washed with DI water and anhydrous ethanol many times before being dried in a 60 °C oven to get white powder.

2.3 Electrospinning of the D-phe@ZnO/P(VDF-TrFE) nanofibers

1 g P(VDF-TrFE) powder was added to a mixed solution of 3.5 mL dimethylformamide and 1.5 mL acetone and then stirred at room temperature for 10 h.

After that, 0.4 g D-phe@ZnO was added and stirred at room temperature overnight to obtain a stable and homogeneous mixture. Correspondingly, the P(VDF-TrFE) and ZnO/P(VDF-TrFE) solutions were generated in the same way as the Dsolutions in the phe@ZnO/P(VDF-TrFE) comparative experiments. electrospinning, a steel cylinder with a diameter of 14 cm was used as the rotary carrier and the aluminum (Al) foil was attached to the steel cylinder outside surface to collect the fibers. The P(VDF-TrFE) solution was ejected at a rate of 0.1 mL/h using a syringe pump. The applied voltage was 15 kV between the nozzle and the Al foil, at a distance of 10 cm. All films were obtained after collecting the fibers for 4 hours with a cylinder speed of 1500 rpm. The electrospinning films were placed in the cylinder at room temperature for 1 h for desiccation.

2.4 Piezoelectric nanogenerator fabrication

All PNGs were fabricated with an effective working area of 2.5× 2.5 cm². The Al foil electrodes were placed on both sides of the fiber mat after the electrospinning film was trimmed to the required proportions. A copper tape was used to adhere to the copper wires that served as test electrodes on both sides. And two Polyimide (PI) substrates were used to package the device, ensuring its longevity in the ambient environment. For photodetector testing, one side electrode of the device was replaced with PET/ITO.

2.5 Measurements and characterization

Morphologies of the ZnO nanoparticles, D-phe@ZnO chelate nanowires and all fibers were characterized by transmission electron microscopy (TEM) (FEI TECNAI G20, FEI, USA) and field emission scanning electron microscopy (FESEM) (JMS 6510LV, JEOL, Japan). Fourier transform infrared (FT-IR) spectroscopy (Nicolet iS50, USA), X-ray diffraction (XRD, Bruker D8 Focus diffractometer, CuK_{α} radiation, Germany) and Raman spectrometer (LabRam HR800, Jobin Yvon, France) were used to characterize ZnO nanoparticles, D-phe@ZnO chelate nanowires, and all fibers. A ferroelectric tester (Precision Premier II, Radiant, USA) was used to determine the polarization-electric field (*P-E*) hysteresis curves of all films. The

dynamic pressing force applied to PNGs was measured using a digital force gauge (Aipu Metrology Instrument Co., Ltd, Zhejiang, China). Short-circuit current and output voltage were measured using a sourcemeter (2450, Keithley, USA) and an oscilloscope (TBS1072B, Tektronix, USA), respectively.

3. Results and discussion

The morphology of pure ZnO nanoparticles and D-phe@ZnO chelate nanowires were imaged with a TEM as shown in Fig. 1(a). Clearly, the size of ZnO nanoparticles was about 30 nm (Fig. 1(a-i, a-ii)). However, the chelate of ZnO and D-phe shows a nanowire structure with a diameter of around 400 nm and a large number of ZnO nanoparticles are attached to the surface of the D-phe@ZnO chelate nanowires (Fig. 1(a-iii, a-iv)). Energy dispersive spectrocopy measurements (EDS) confirmed the uniform distribution of C, N, O in D-phe and the attachment of ZnO nanoparticles to the surface of the nanowire, as shown in Fig. 1(b). The dendritic structure can be seen on both ends of the nanowires, as shown in the inset of Fig. 1(a-iii). It is clearly observed in the photographs in Fig. 1(b) that D-phe@ZnO chelate nanowires have a better dispersibility compared to pure ZnO nanoparticles. One can see that pure ZnO nanoparticles aggregate and precipitate after holding for 30 minutes in deionized water. The crystallographic structure of the two samples was investigated by XRD analysis. All of the diffraction characteristic peaks are assigned to the crystallinity of ZnO, as illustrated in Fig. 2(a), which is in line with the standard JCPDS card (No. 75-0576). In addition, the ZnO in both samples shows a wurtzite structure, and the addition of D-phe does not change the crystal phase of ZnO.

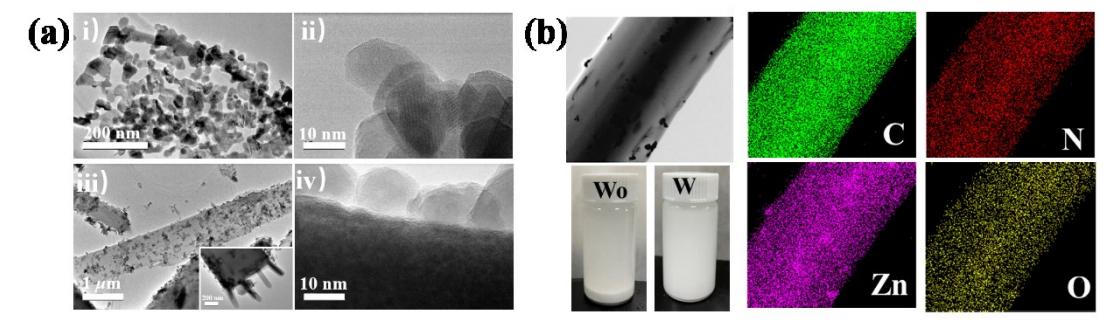


Fig. 1. (a) TEM images of (i, ii) ZnO nanoparticles and (iii, iv) D-phe@ZnO chelate nanowires, the inset of (iii) is a TEM image showing the dendric end of a D-phe@ZnO chelate nanowire. (b) TEM and the corresponding EDS mapping images of a single D-phe@ZnO chelate nanowire. The

two photographs show the dispersion of ZnO in deionized water with and without D-phe.

FT-IR analysis was carried out to determine the functional group alterations before and after chelation. The FT-IR spectra of the D-phe and the D-phe@ZnO chelate nanowires were analyzed, and many discrepancies were found in Fig. 2(b). For D-phe (black line), the broad, strong band between 3100-2800 cm⁻¹ and the broad, weak band in the range of 2600-2200 cm⁻¹ were attributed to the stretching vibration of the NH₃⁺ groups. The broad band at 2123 cm⁻¹ confirmed the antisymmetric deformation vibration and the hindered internal rotation of the NH₃⁺ groups. A sharp peak at 1307 cm⁻¹ was attributed to the C-OH vibration. However, these peaks seem to disappear in the D-phe@ZnO (red line) nanowires. Because of the weakly alkaline buffer solution formed by Tris, the C-OH vibration peak disappeared, indicating that the carboxylic acid group in D-phe has been deprotonated into a carboxylate ion¹⁹. The vibrational mode of C=O is coupled to another oxygen due to the deprotonation of the carboxylic group. As a result, the COO symmetric and asymmetric stretching vibration peaks were formed, focusing on the 1622 cm⁻¹ and 1408, 1390 cm⁻¹ peak, respectively. On the other hand, the H⁺ ions from NH₃⁺ groups of the D-phe were neutralized by OH⁻ ions and the NH₂ groups were easy to obtain, which corresponded to the symmetric and asymmetric stretching vibration of N-H bonds in NH2 groups at 3258 and 3334 cm⁻¹ in the spectra. A new broad peak around 438 cm⁻¹ was attributable to the vibration in ZnO. Based on FT-IR results, it can be confirmed that Zn²⁺ of ZnO was chelated with the carboxylate group.

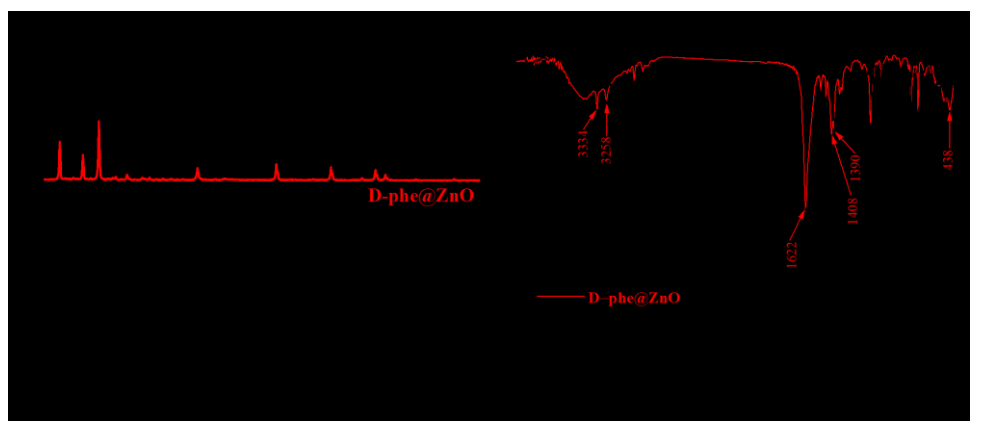


Fig. 2. (a) XRD patterns of ZnO and D-phe@ZnO. (b) FT-IR spectra of D-phe and D-phe@ZnO.

The fine chemical structure of ZnO, D-phe, and D-phe@ZnO chelate nanowires

were also determined using XPS. A sharp peak located at 398.4 eV was observed by introducing D-phe, corresponding to the 1s peak of the nitrogen element in the widescan XPS spectra in Fig. 3(a). The N 1s spectra of D-phe was split into two peaks, as shown in Fig. 3(b), in which the peaks at 400.2 and 397.9 eV can be attributed to the NH₃⁺and NH₂, respectively. However, the N 1s spectra of D-phe@ZnO chelate nanowires were only one peak associated with NH₂ at 398.4 eV, as shown in Fig. 3(c). These spectra confirmed that NH₃⁺ is deprotonated into NH₂, in agreement with FT-IR results. On the other hand, the O 1s spectra of ZnO in Fig. 3(d) can be split into two peaks at 531.0 and 532.1 eV, which corresponds to the lattice oxygen in ZnO and the surface absorbed -OH, respectively. In the O 1s spectra for D-phe in Fig. 3(e), there are two peaks at 530.3 and 532.0 eV, corresponding to COO- and -OH, respectively. More importantly, in D-phe@ZnO chelate in Fig. 3(f), the O 1s spectrum can be deconvoluted into three peaks at 529.3, 531.0, and 532.2 eV, which corresponds to the oxygen in ZnO, COO-, and -OH groups, respectively. The O 1s peak for ZnO shifted to low binding energy, whereas the O 1s peak for COO-shifted to the high binding energy. The relative shifts of the two peaks provided strong evidence for the chelation of Zn²⁺ and COO⁻. Meanwhile, the Zn 2p peak for D-phe@ZnO chelate nanowires shifted to low binding energy as shown in Fig. S1(a). Based on the observed results, it was believed that the COO group in D-phe was chelated with zinc ions in ZnO nanoparticles,²⁰ and thus forming the chelated nanowires, as in the schematic chelate structure in Fig. S1(b).

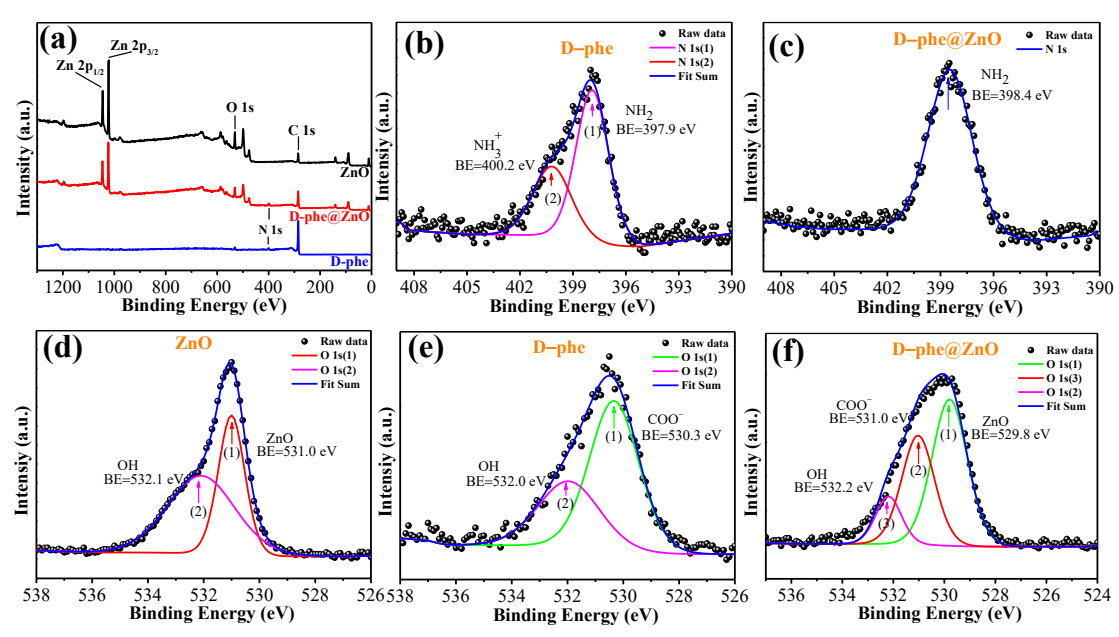


Fig. 3. XPS spectra of (a) ZnO, D-phe, and D-phe@ZnO, N1s deconvoluted peaks of (b) D-phe, and (c) D-phe@ZnO, O1s deconvoluted peaks of (d) ZnO, (e) D-phe, and (f) D-phe@ZnO.

Figure 4(a-c) shows the SEM images of the P(VDF-TrFE) fibers, ZnO/P(VDF-TrFE) fibers and D-phe@ZnO/P(VDF-TrFE) fibers, for convenience, we abbreviate them as P, ZP and DZP, respectively. The orientation distribution of the nanofibers was statisticalized by using the ImageJ software. The angle distribution for P nanofibers was in the range of -20°~20° (Fig. S2(a)). The ZP nanofibers showed multiple beads in each nanofiber due to the aggregation of the ZnO nanoparticles as shown in Fig. 3(b). Although the angle distribution range is -20°~20° (Fig. S2(b)), one can see that the arrangement of nanofibers becomes sparse. Whereas, the DZP nanofibers show highly ordered, straight and tightly arranged features as shown in Fig. 4(c). A narrow-angle distribution around 0~20° (Fig. S2(c)) confirms the highly aligned nanofiber structure. Due to multi-level-oriented structures in this system, such as alignment of dipoles, molecule chain, and fibers, highly aligned nanofibers exhibit a low-entropy structure²¹. The D-phe@ZnO nanowires embedded in the P(VDF-TrFE) nanofibers were clearly visible in the SEM image in Fig. S2(d). EDS mapping images confirmed that the D-phe@ZnO nanowire was well embedded in the P(VDF-TrFE) nanofibers forming a coaxial structure. In order to better explain that the nanofibers become straight and dense, the mechanism diagram was shown in Fig. S3 in the supporting information. For pure P(VDF-TrFE) precursors, in far-field

electrostatic spinning, the syringe needle was far from the collector drum, while the weak charging ability of P(VDF-TrFE) with low dielectric constant causes P(VDF-TrFE) nanofibers to drift with the electric field resulting in bended and loose aligned nanofibers. However, when high dielectric constant D-phe@ZnO nanowires were added, they acted as additional electrodes due to their high charging capacity and split the far electric field into many near electric fields. These near electric fields forced the nanofibers well-aligned and compacted dense with each other. Thus, the nanofibers were stable on the surface of the collecting drum, resulting in highly oriented and dense nanofiber films.

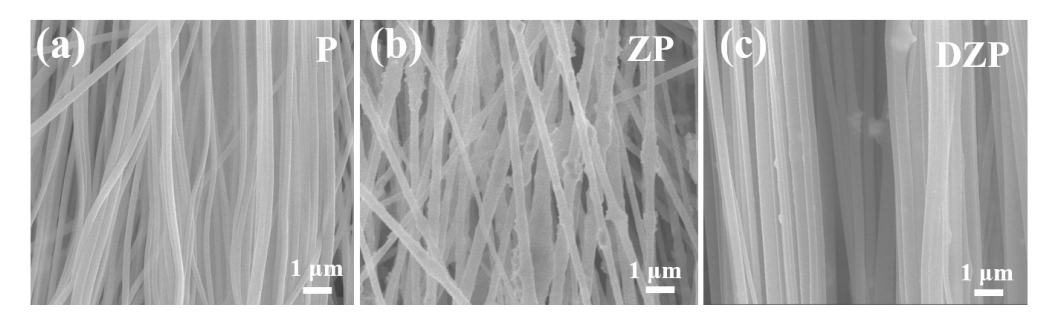


Fig. 4. SEM image of (a) pure P(VDF-TrFE) nanofibers, (b) ZnO/P(VDF-TrFE) nanofibers and (c) D-phe@ZnO/P(VDF-TrFE) nanofibers.

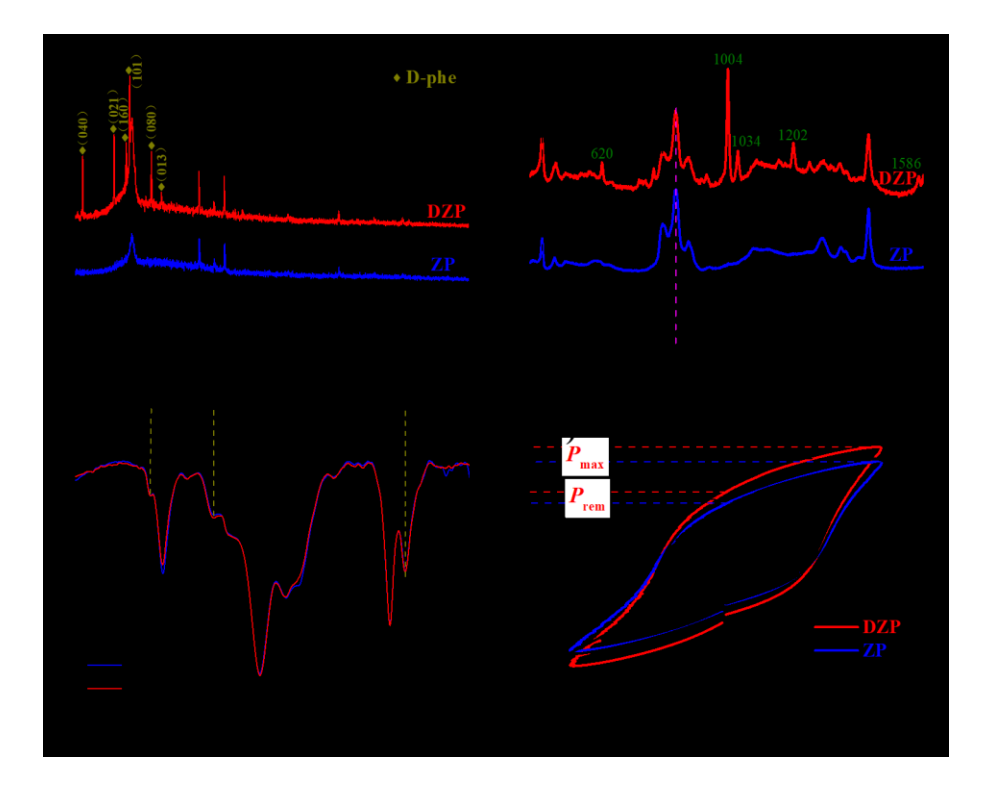


Fig. 5. (a) XRD patterns, (b) Raman spectra, (c) FT-IR spectra and (d) P-E loops of P, ZP, and DZP nanofibers, respectively.

The results of the XRD characterization of the P, ZP, and DZP nanofibers are shown in Fig. 5(a). The XRD pattern of the DZP shows a sharp peak at 19.8°, which corresponds to the (110/200) plane of the β-phase, while the others (i.e., P and ZP nanofibers) show a relatively weak peak at 19.8°. The diffraction peaks of ZnO and D-phe can be observed in the pattern of DZP. The Raman spectra of all synthesized samples were shown in Fig. 5(b). The 805 cm⁻¹ vibrational band was caused by CH₂ bond rocking, which was associated with the non-polar α-phase. Raman peak at 840 cm⁻¹ due to CH₂ rocking, CF₂ stretching and skeletal C-C stretching represent polarized β -phase in the samples²². In the spectrum of DZP, the band at 620 cm⁻¹ can be defined as the breathing vibrations of the phenyl ring. The band at 1004 cm⁻¹ was derived from the phenyl ring angular bending vibrations. The peak at 1034 cm⁻¹ was from the synchronized movement of C-C-H and C-C. The band at 1202 cm⁻¹ was mainly attributed to the side chain $(C_{\beta}-C_{\gamma})$ vibration. The peak at 1586 cm⁻¹ was also from bond-stretching vibrations of the phenyl ring ²³. A strong Raman band at 847 cm⁻¹ was associated with the β-phase in the DZP spectra. The FT-IR spectra of all nanofibers were shown in Fig. 5(c) to further illustrate the polar crystalline phase (βphase). The absorbance peaks are found at 847, 1282, and 1428 cm⁻¹, which illustrates the peaks belong to the β-phase. The non-polar α-phase bands (765, 796, 854, 870, and 970 cm⁻¹) were not obvious, indicating that electrospinning was a quick and easy way to generate the polar β-phase of P(VDF-TrFE) nanofibers. P(VDF-TrFE) contains a lot number of Fluorine (F) atoms with a larger diameter than that of hydrogen atoms, which will cause large steric effects and make it easier for P(VDF-TrFE) to form the β -phase²⁴. Therefore, the vibration intensity of the β -phase of the DZP nanofibers (red line) is higher than that of P and ZP. The polarization-electric field (P-E) hysteresis loops of all nanofiber films were measured to describe the ferroelectricity, as shown in Fig. 5(d). All of the nanofibers exhibited typical hysteresis loops with relatively large remnant polarization (P_r) values. The coercive field of three samples was almost the same, all of which were 23 MV/m. The maximum polarization (P_{max}) value of DZP was increased to 5.23 μ C/cm² compared to 4.52 μ C/cm² of ZP and 4.66 μ C/cm² of P. We can find that the P_{max} of ZP is also

reduced compared to that of P. The same variation trend was also observed in the $P_{\rm r}$ values of the three samples, increasing from 2.65 μ C/cm² (P) to 3.06 μ C/cm² (DZP). Proving that DZP nanofibers have a better Ferroelectricity.

The piezoelectric performance of PNGs was tested on a specialized platform in a repeated tapping mode, which can provide periodic pressure about 10 N at 2 Hz by a 2 cm diameter cylinder. Figure 6 shows the outputs of PNG assembled by P (P-PNG), ZP (ZP-PNG), and DZP (DZP-PNG) nanofibers in the forward connection and reverse connection. The P-PNG, ZP-PNG, and DZP-PNG generated voltage of 9.5 V, 16.2 V, 21.8 V and current of 1.4 μA, 2.8 μA, 4.1 μA, respectively, as shown in Fig.6(a, d). Compared with the P-PNG with pure P(VDF-TrFE), the DZP-PNG using D-phe@ZnO nanowires has a great improvement in output voltage and current. Since the mass percentage of ZnO was not changed, this improvement is mainly due to the improvement in the quality of the nanofiber film. Next, the output signals of DZP-PNG were measured under the forward and reverse connection, as shown in Fig. 6(b, e). To observe the difference between forward and reverse connections more clearly, Figures 6 (c, f) select the output voltage and current for an individual cycle, and it can be easily observed that the voltage and current were generated and the direction is opposite when pressing and releasing.

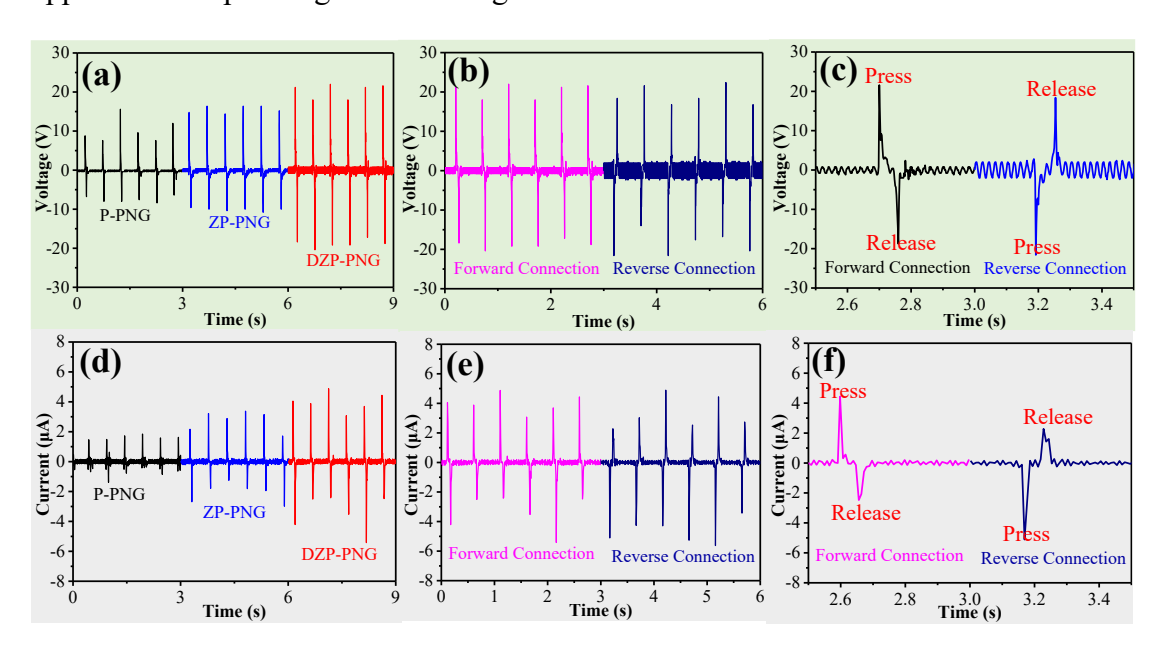


Fig. 6. The output voltage of (a) P-PNG, ZP-PNG, and DZP-PNG, (b) forward and reverse connection under tapping mode, and (c) one cycle of forward and reverse connection. The output

current of (d) P-PNG, ZP-PNG, and DZP-PNG, (e) forward and reverse connection, and (f) one cycle of forward and reverse connection.

As shown in Fig. 7(a), the load voltage and power density of the DZP-PNG were investigated by connecting the various external resistances ranging from 510 k Ω to 1 GΩ. Figure S4 (a) shows the detailed output voltages of DZP-PNG with various load resistances. The load voltage increased as the load resistance increased, reaching a saturated value of around 33 V at the load resistance of 1 G Ω (black line). In other words, the open-circuit voltage of DZP-PNG was 33 V. Meanwhile, at a resistance of 10 M Ω , the DZP-PNG can achieve a maximum output power density of about 8.5 μW/cm². As shown in Table 1, compared with the previous work, the performance of this PNG has been greatly improved. To illustrate the practical application of the asprepared DZP-PNG, using a bridge rectifier, only positive signals were observed in Fig. 7(b). Figure 7(c) shows the piezoelectric converted electrical energy rectified and stored in various capacitors. The black curve reveals that it takes only 13 s, just 26 cycles, for DZP-PNG to charge the 1 µF capacitor to 2 V. Inset of Fig. 7(c) shows a photograph of the DZP-PNG. It can be noticed that the output voltage signals of the PNG increased with the increase of the repetitive tapping process, as shown in Fig. 7(d), which was attributed to an increase in the real contact area between the nanofibers due to the rapidly compressed of nanofibers at the beginning of repeated tapping. The durability and reliability of the PNGs were demonstrated by the repetitive tapping for 7200 cycles with a repeating rate of 2 Hz. As shown in Fig. S4(b), almost no decline of the output voltages is observed over a long period of 7200 cycles. The PNG energy harvesting ability was also confirmed by small body motions such as finger tapping, as shown in Fig. 7(e, f). Whether it was tapping slowly or quickly, the PNG presented a stable voltage output of about 25 V. Remarkably, as presented in the inset of Fig. 7(e), the PNG directly drove 15 commercial LEDs without any charge storage.

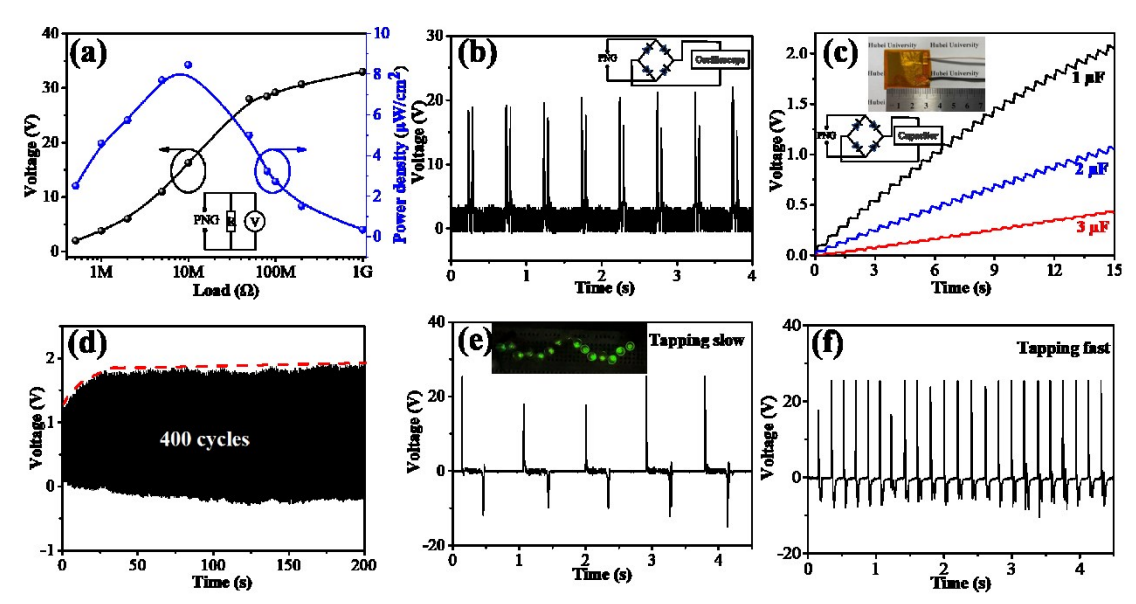


Fig. 7. (a) Output voltage and corresponding power density and (b) output rectified voltages of DZP-PNG. (c) The different capacitor charging voltages of DZP-PNG in the rectification system. The insert of (c) is a photograph of the flexible DZP-PNG. (d) 400 cycles durability test results of DZP-PNG. The output voltage of (e) tapping slow and (f) tapping fast by finger. The insert of (e) is that 15 commercial LEDs are directly lighted up by the DZP-PNG without using storage capacitors.

Table 1. Performance of P(VDF-TrFE) based piezoelectric generators with different materials.

Piezoelectric materials	Preparation mehods	Voltage (V)	Power density (µW/cm²)	Ref.
P(VDF-TrFE)	Electrospinning	12	0.16	25
P(VDF-TrFE)	Electrospinning	5	0.8	26
ZnO/P(VDF-TrFE)	Electrospinning	2.65		27
BaTiO ₃ /PVDF-HFP	Electrospinning	12		28
BaSrTiO ₃ /P(VDF-TrFE)	Electrospinning	12		29
D-phe@ZnO/P(VDF-TrFE)	Electrospinning	33	8.5	This work

In order to demonstrate the potential applications in harvesting energy from human movements as a flexible PNG, we used a homemade bending system to measure the output of PNGs. The schematic of a fully bending cycle is plotted in Fig. 8(a). In the bending mode, films were bent into an arch, and the radius R of curvature of the arch decreases as the slider moves further away. The following equation can be used to determine the bending strain ε imposed on the film:³⁰

$$\varepsilon = \frac{h_{sub} + h_P}{2R} \tag{1}$$

where h_{sub} is the thicknesses of the substrate, and h_{P} is the thicknesses of P(VDF-TrFE) film. R can be estimated by matching an inscribed circle to the arch's apex, as illustrated in Fig. 8(b). According to the above formula, ε_{max} is 2% when R_{min} is 1 cm in our experiments. Figures 8(c, d) are the voltage output of PNG in the bending

experiment. PNG can produce an output voltage of 6 V under a relatively small bending strain of 2%. The video S1 shows the signal of the oscilloscope during the bending process in the supporting information. When the device is attached to the knee, a voltage of \sim 3 V can be generated when it is bent, and a voltage of \sim -3 V can be generated by getting flat. These results indicate the potential value of PNGs in wearable devices.

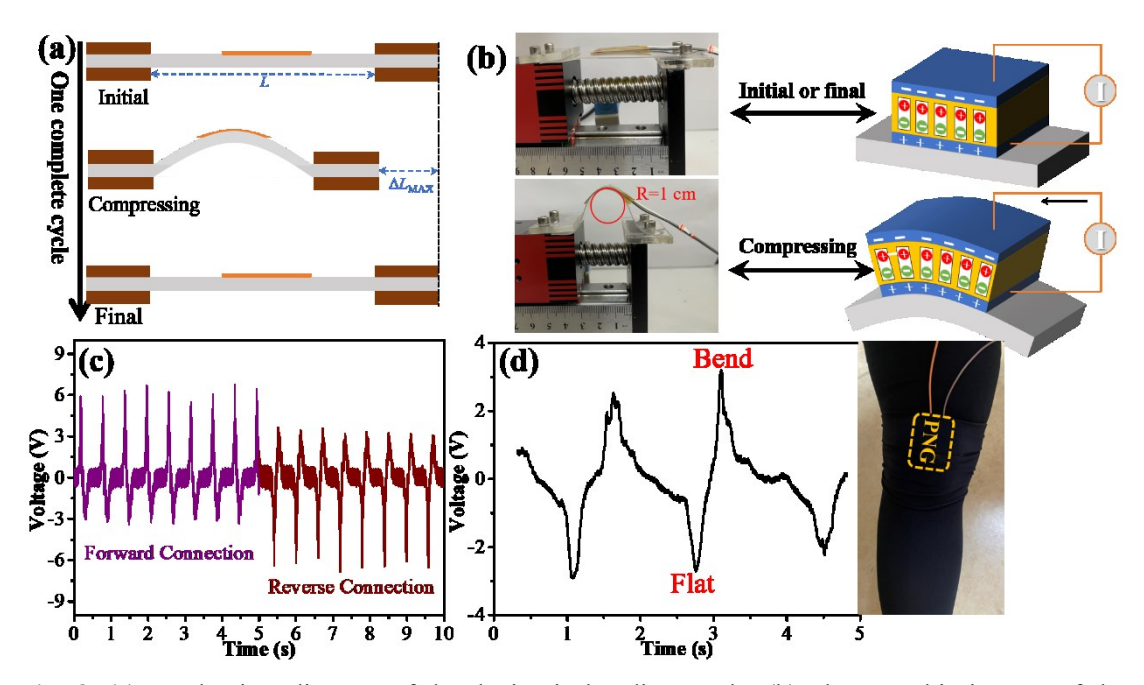


Fig. 8. (a) Mechanism diagram of the device in bending mode. (b) Photographic images of the devices attached to a measuring station without bending or with bending, the corresponding mechanism diagram on the right panel. (c) Output voltages from bending mode of forward and reverse connection. (d) Photograph of PNG attached to the knee and corresponding voltage output during walking.

Furthermore, the photo-response behaviors of D-phe@ZnO were ensured by the UV-visible absorption as shown in Fig. S5. It can be found that ZnO and D-phe@ZnO exhibit intense absorption around 390 nm, indicating the UV photoresponse of the composite nanofibers. Figure 9(a, b) shows the current-voltage (*I-V*) and current-time (*I-t*) characteristics of the photodetectors assembled by DZP films under dark and 365 nm UV illumination. It is obvious that the photocurrent increases immediately when the film is exposed to UV light illumination. With the increase of UV light power, the current increases significantly. This proves that the DZP film can detect UV light power. Thus, a photoactive piezoelectric nanogenerator has been prepared by replacing the Al electrode with a transparent flexible ITO electrode coated PET as

illustrated in Fig 9(c). Combining the different UV power density illumination, the electrical outputs of the DZP-PNG under periodic stress are shown in Fig. 9(d). Under UV light illumination, the average peak value of the open-circuit voltage decreases compared with that in dark conditions. And with the increase of UV light power density, the output voltage of the device gradually decreases, showing the ability of UV photodetection. Under UV light illumination, photocurrent generated by photogenerated extra carriers within the sample leads to an enhancement of the short-circuit current. One infers that the photogenerated carriers could screen the piezoelectric charges and thus reduce the open voltage³¹. The bifunctional response of the DZP-PNG indicates its potential in the application for self-powered flexible visible UV light detector/sensor.

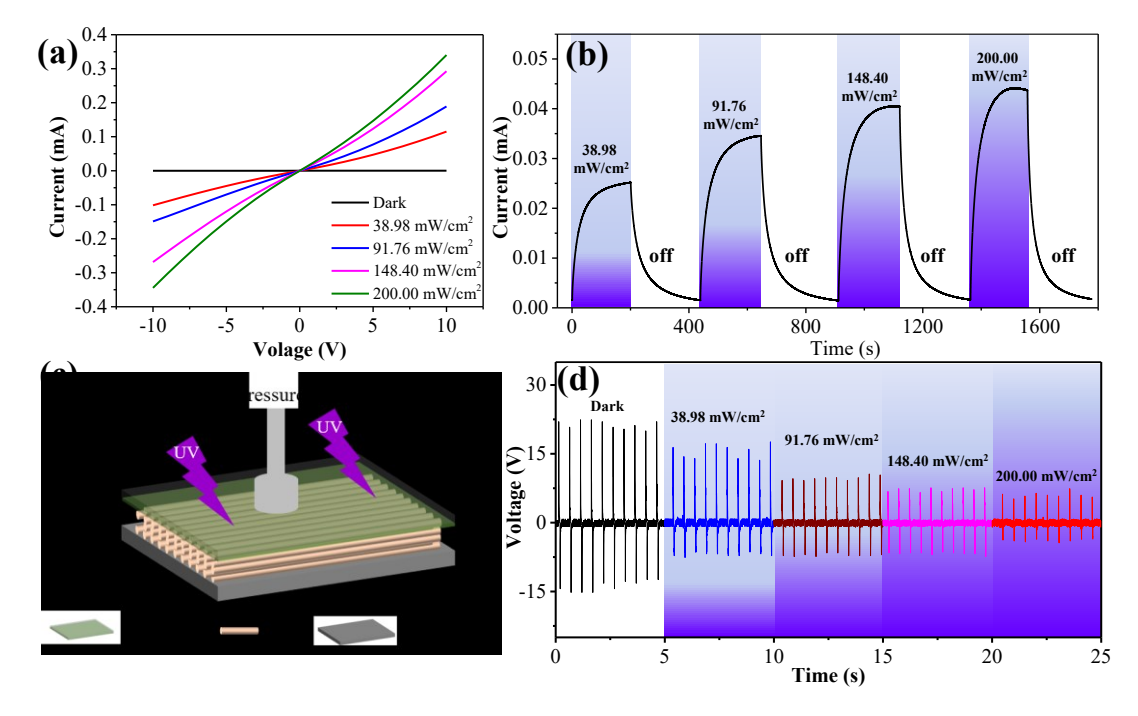


Fig. 9. (a) Current-voltage characteristics and (b) current-time curves of DZP nanofiber film under different UV power density light illumination. (c) Schematic of DZP-PNG operation under concurrent tapping and UV light. (d) The output voltage under different UV power density light illumination.

4. Conclusions

In summary, highly oriented and densely arranged P(VDF-TrFE) nanofiber-based composite mats have been prepared by introducing well dispersed D-phe@ZnO chelate nanowires. The low-entropy structure improved the orientation and

compaction of the nanofiber mats and thereby enhanced the electrical output performance. The newly designed PNG possessed an energy harvesting ability with a maximum output voltage of 33 V, a short-circuit current of about 4.1 µA, and a power density of 8.5 µW/cm². Meanwhile, 6 V voltage output can also be obtained in a bending test. High voltage outputs can be obtained both in the bending and tapping mode with body movements. Furthermore, the composite films exhibit powerful properties of UV light absorption as well, confirming the promising applications as a self-powered photodetector. The coupling of the UV photosensitive ZnO with P(VDF-TrFE) guarantees the detection of UV light by changing the piezoelectric output voltages and currents. All these prove that the device has broad application prospects in wearable electronic devices and self-powered devices.

ASSOCIATED CONTENT

Supporting Information

XPS spectra of Zn 2p; chemical structure of D-phe@ZnO chelate nanowires; distribution angle range; TEM and the corresponding EDS mapping images; mechanism diagram of the formation of aligned DZP nanofibers; output voltage under different external load resistance; 7200 cycles durability test results of DZP-PNG; UV-vis absorption spectra of pure ZnO and D-phe@ZnO; bending video.

Acknowledgments

This work was financially supported by the National Natural Science Foundation of China (No. 11974104 and No. 12104137) and this work also thanks to the support from the Program of Introducing Talents of Discipline to Universities ("111 Project", No. D18025) China. Dr. C. W. Huang thanks the support from Hubei Key Laboratory of Polymer Materials, Hubei University.

References

- 1. Chu, S.; Majumdar, A., Opportunities and challenges for a sustainable energy future. *Nature* **2012**, *488* (7411), 294-303.DOI: 10.1038/nature11475.
- 2. Ates, H. C.; Yetisen, A. K.; Güder, F.; Dincer, C., Wearable devices for the detection of COVID-19. *Nature Electronics* **2021**, 4 (1), 13-14.DOI: 10.1038/s41928-020-00533-1.
- 3. Smarr, B. L.; Aschbacher, K.; Fisher, S. M.; Chowdhary, A.; Dilchert, S.; Puldon, K.; Rao, A.; Hecht, F. M.; Mason, A. E., Feasibility of continuous fever monitoring using wearable devices. *Scientific Reports* **2020**, *10* (1), 21640.DOI: 10.1038/s41598-020-78355-6.
- 4. Moon, J. H.; Kang, M.-K.; Choi, C. E.; Min, J.; Lee, H. Y.; Lim, S., Validation of a wearable cuff-less wristwatch-type blood pressure monitoring device. *Scientific Reports* **2020**, *10* (1), 19015.DOI: 10.1038/s41598-020-75892-y.
- 5. Lee, J. H.; Kim, H.; Hwang, J.-Y.; Chung, J.; Jang, T.-M.; Seo, D. G.; Gao, Y.; Lee, J.; Park, H.; Lee, S. J., 3D Printed, Customizable, and Multifunctional Smart Electronic Eyeglasses for Wearable Healthcare Systems and Human–Machine Interfaces. *ACS applied materials & interfaces* **2020**, *12* (19), 21424-21432.DOI:
- 6. Karan, S. K.; Maiti, S.; Lee, J. H.; Mishra, Y. K.; Khatua, B. B.; Kim, J. K., Recent Advances in Self-Powered Tribo-/Piezoelectric Energy Harvesters: All-In-One Package for Future Smart Technologies. *Advanced Functional Materials* **2020**, *30* (48), 2004446.DOI: 10.1002/adfm.202004446.
- 7. Wang, Z. L., Self-Powered Nanosensors and Nanosystems. *Advanced Materials* **2012**, *24* (2), 280-285.DOI: 10.1002/adma.201102958.
- 8. Xu, S.; Qin, Y.; Xu, C.; Wei, Y.; Yang, R.; Wang, Z. L., Self-powered nanowire devices. *Nature Nanotechnology* **2010**, *5* (5), 366-373.DOI: 10.1038/nnano.2010.46.
- 9. Qin, W.; Zhou, P.; Qi, Y.; Zhang, T., Lead-Free Bi_{3.15}Nd_{0.85}Ti₃O₁₂ Nanoplates Filler-Elastomeric Polymer Composite Films for Flexible Piezoelectric Energy Harvesting. *Micromachines (Basel)* **2020**, *11* (11), 966.DOI: 10.3390/mi11110966.
- 10. Wang, Z. L., Nanogenerators, self-powered systems, blue energy, piezotronics and piezophototronics A recall on the original thoughts for coining these fields. *Nano Energy* **2018**, *54*, 477-483.DOI: 10.1016/j.nanoen.2018.09.068.

- 11. Qin, W.; Zhou, P.; Xu, X.; Irshad, M. S.; Qi, Y.; Zhang, T., Enhanced output performance of piezoelectric energy harvester based on hierarchical Bi_{3.15}Nd_{0.85}Ti₃O₁₂ microspheres/PVDF-HFP composite. *Sensors and Actuators A: Physical* **2022**, *333*, 113307.DOI: 10.1016/j.sna.2021.113307.
- 12. Shi, K.; Huang, X.; Sun, B.; Wu, Z.; He, J.; Jiang, P., Cellulose/BaTiO₃ aerogel paper based flexible piezoelectric nanogenerators and the electric coupling with triboelectricity. *Nano Energy* **2019**, *57*, 450-458.DOI: 10.1016/j.nanoen.2018.12.076.
- 13. Yao, Z.; Song, Z.; Hao, H.; Yu, Z.; Cao, M.; Zhang, S.; Lanagan, M. T.; Liu, H., Homogeneous/Inhomogeneous-Structured Dielectrics and their Energy-Storage Performances. *Advanced Materials* **2017**, *29* (20), 1601727.DOI: 10.1002/adma.201601727.
- 14. Yang, K.; Huang, X.; Zhu, M.; Xie, L.; Tanaka, T.; Jiang, P., Combining RAFT Polymerization and Thiol–Ene Click Reaction for Core–Shell Structured Polymer@BaTiO₃ Nanodielectrics with High Dielectric Constant, Low Dielectric Loss, and High Energy Storage Capability. *ACS Applied Materials & Interfaces* **2014**, *6* (3), 1812-1822.DOI: 10.1021/am4048267.
- 15. de Vries, W. C.; Tesch, M.; Studer, A.; Ravoo, B. J., Molecular Recognition and Immobilization of Ligand-Conjugated Redox-Responsive Polymer Nanocontainers. *ACS Applied Materials & Interfaces* **2017**, *9* (48), 41760-41766.DOI: 10.1021/acsami.7b15516.
- 16. Tahir, M. N.; Zink, N.; Eberhardt, M.; Therese, H. A.; Kolb, U.; Theato, P.; Tremel, W., Overcoming the Insolubility of Molybdenum Disulfide Nanoparticles through a High Degree of Sidewall Functionalization Using Polymeric Chelating Ligands. *Angewandte Chemie International Edition* **2006**, *45* (29), 4809-4815.DOI: 10.1002/anie.200504211.
- 17. Sun, Z.; Sun, B.; Qiao, M.; Wei, J.; Yue, Q.; Wang, C.; Deng, Y.; Kaliaguine, S.; Zhao, D. J., A general chelate-assisted co-assembly to metallic nanoparticles-incorporated ordered mesoporous carbon catalysts for Fischer–Tropsch synthesis. *Journal of the American Chemical Society* **2012**, *134* (42), 17653-17660.DOI: 10.1021/ja306913x.
- 18. Sultana, A.; Sadhukhan, P.; Alam, M. M.; Das, S.; Middya, T. R.; Mandal, D., Organolead halide perovskite induced electroactive β-phase in porous PVDF films: an excellent material for photoactive piezoelectric energy harvester and photodetector. *ACS applied materials & interfaces* **2018**, *10* (4), 4121-4130.DOI: 10.1021/acsami.7b17408

- 19. Saifullah, B.; Hussein, M. Z.; Hussein-Al-Ali, S. H.; Arulselvan, P.; Fakurazi, S., Sustained release formulation of an anti-tuberculosis drug based on para-amino salicylic acid-zinc layered hydroxide nanocomposite. *Chemistry Central Journal* **2013**, *7* (1), 72.DOI: 10.1186/1752-153X-7-72.
- 20. Yao, Y.; Hou, H.; Liu, X.; Yu, C.; Li, D.; Dai, Z. J. S. I., Zinc l-phenylalanine chelate nanofiber anode in lithium ion battery. *Surface Innovations* **2018**, *7* (1), 27-35.DOI: 10.1680/jsuin.18.00041
- 21. Tang, C.-Y.; Zhao, X.; Jia, J.; Wang, S.; Zha, X.-J.; Yin, B.; Ke, K.; Bao, R.-Y.; Liu, Z.-Y.; Wang, Y.; Zhang, K.; Yang, M. B.; Yang, W., Low-entropy structured wearable film sensor with piezoresistive-piezoelectric hybrid effect for 3D mechanical signal screening. *Nano Energy* **2021**, *90*.DOI: 10.1016/j.nanoen.2021.106603.
- 22. Arrigoni, A.; Brambilla, L.; Bertarelli, C.; Serra, G.; Tommasini, M.; Castiglioni, C., P(VDF-TrFE) nanofibers: structure of the ferroelectric and paraelectric phases through IR and Raman spectroscopies. *RSC Advances* **2020**, *10* (62), 37779-37796.DOI: 10.1039/d0ra05478j.
- 23. Hernández, B.; Pflüger, F.; Kruglik, S. G.; Ghomi, M. J. J. o. R. S., Characteristic Raman lines of phenylalanine analyzed by a multiconformational approach. *Journal of Raman Spectroscopy* **2013**, *44* (6), 827-833.DOI: 10.1002/jrs.4290
- 24. Fukada, E., History and recent progress in piezoelectric polymers. *IEEE Transactions on Ultrasonics, Ferroelectrics, and Frequency Control* **2000,** 47 (6), 1277-1290.DOI: 10.1109/58.883516.
- 25. You, S.; Zhang, L.; Gui, J.; Cui, H.; Guo, S., A Flexible Piezoelectric Nanogenerator Based on Aligned P(VDF-TrFE) Nanofibers. *Micromachines* **2019**, *10* (5).DOI: 10.3390/mi10050302.
- 26. Gui, J.; Zhu, Y.; Zhang, L.; Shu, X.; Liu, W.; Guo, S.; Zhao, X., Enhanced output-performance of piezoelectric poly(vinylidene fluoride trifluoroethylene) fibers-based nanogenerator with interdigital electrodes and well-ordered cylindrical cavities. *Applied Physics Letters* **2018**, *112* (7), 072902.DOI: 10.1063/1.5019319.
- 27. Li, J.; Zhao, C.; Xia, K.; Liu, X.; Li, D.; Han, J., Enhanced piezoelectric output of the PVDF-TrFE/ZnO flexible piezoelectric nanogenerator by surface modification. *Applied Surface Science* **2019**, *463*, 626-634.DOI: 10.1016/j.apsusc.2018.08.266.
- 28. Dhakras, D.; Ogale, S., High-Performance Organic-Inorganic Hybrid Piezo-Nanogenerator

- via Interface Enhanced Polarization Effects for Self-Powered Electronic Systems. *Advanced Materials Interfaces* **2016**, *3* (20), 1600492.DOI: 10.1002/admi.201600492.
- 29. An, S.; Jo, H. S.; Li, G.; Samuel, E.; Yoon, S. S.; Yarin, A. L., Sustainable Nanotextured Wave Energy Harvester Based on Ferroelectric Fatigue-Free and Flexoelectricity-Enhanced Piezoelectric P(VDF-TrFE) Nanofibers with BaSrTiO₃ Nanoparticles. *Advanced Functional Materials* **2020**, *30* (25), 2001150.DOI: 10.1002/adfm.202001150.
- 30. Yang, J.; Chen, Q.; Xu, F.; Jiang, H.; Liu, W.; Zhang, X.; Jiang, Z.; Zhu, G. J. A. E. M., Epitaxy Enhancement of Piezoelectric Properties in P (VDF-TrFE) Copolymer Films and Applications in Sensing and Energy Harvesting. *Advanced Electronic Materials* **2020**, *6* (10), 2000578.DOI: 10.1002/aelm.202000578
- 31. Sultana, A.; Sadhukhan, P.; Alam, M. M.; Das, S.; Middya, T. R.; Mandal, D., Organo-Lead Halide Perovskite Induced Electroactive β-Phase in Porous PVDF Films: An Excellent Material for Photoactive Piezoelectric Energy Harvester and Photodetector. *ACS Applied Materials & Interfaces* **2018**, *10* (4), 4121-4130.DOI: 10.1021/acsami.7b17408.

Table of Contents Graphic

